Thermodynamic modeling of binary phase diagram of 2-amino-2-methyl-1, 3-propanediol and TRIS(hydroxymethyl)aminomethane system with experimental verification

ARTICLE *in* CALPHAD · JUNE 2015

Impact Factor: 1.37 · DOI: 10.1016/j.calphad.2015.05.003

CALPHAD: Computer Coupling of Phase Diagrams and Thermochemistry 50 (2015) 126–133

Contents lists available at ScienceDirect

CALPHAD: Computer Coupling of Phase Diagrams and Thermochemistry

journal homepage: www.elsevier.com/locate/calphad

Thermodynamic modeling of binary phase diagram of 2-amino-2-methyl-1, 3-propanediol and TRIS(hydroxymethyl)aminomethane system with experimental verification

Prathyusha Mekala [a], Vamsi Kamisetty [b], Wen-Ming Chien [b], Renhai Shi [b], Dhanesh Chandra [b,*], Jitendra Sangwai [a,*], Anjali Talekar [b], Amrita Mishra [c]

[a] Petroleum Engineering Program, Indian Institution of Technology, Madras, India 600036
[b] Chemical and Materials Engineering, University of Nevada, Reno, NV 89557, USA
[c] Department of Mechanical Engineering, University of Mississippi, University, MS 38677 USA

ARTICLE INFO

Article history:
Received 29 January 2015
Received in revised form
28 May 2015
Accepted 29 May 2015
Available online 15 June 2015

Keywords:
Organic thermal energy storage materials
Solid–Solid state phase transformations
Binary phase diagram

ABSTRACT

An experimental binary phase diagram of 2-Amino-2-methyl-1, 3-propanediol (AMPL)-tris(hydroxymethyl)aminomethane (TRIS) is developed by using high temperature in-situ X-ray diffraction (XRD), differential scanning calorimetry (DSC), and thermodynamics modeling. The organic thermal energy storage materials, such as AMPL and TRIS, undergo a solid–solid state phase transition storing large amounts of thermal energy in O–H…O and O–H…N bond rotation. High temperature in-situ XRD and DSC experiments are used to study binary equilibrium AMPL-TRIS phase diagram. Binary solid solutions of AMPL and TRIS exhibit an orientationally disordered BCC structure, in which thermal energy is stored. A computer developed AMPL-TRIS phase diagram by CALPHAD methodology agrees reasonably well with the experimental one. Gibbs energies of pure components were described based on their heat capacity data. The Gibbs energies of metastable phase modifications were establisded by assuming ideal solutions of the phases. The excess Gibbs energy parameters were optimized using Parrot program of Thermo-Calc software to include the experimental data. The phase diagram consists of 5 single phase regions, low temperature α AMPL-rich Monoclinc phase ($P2_1/n$), β-TRIS rich orthorhombic phase, ($Pn2_1a$), γ-AMPL rich and γ' –TRIS rich, both BCC orientationally disordered phases and Liquid phase. There are six two phase regions: (α+β), (β+γ), (β+γ'), (γ+γ'), (L+γ), and (L+γ'). A low temperature eutectoid transformation is observed with invariant point 348 K and 12%TRIS. As the temperature is increased, another higher temperature eutectoid transformation is observed with invariant point 388 K and 54%TRIS. A peritectoid transformation is also observed with invariant point 401 K and 38%TRIS.

1. Introduction

Orientationally disordered organic crystals store large amount of thermal energy during solid state phase transitions, unlike other phase change materials that store energy during solid to liquid phase transitions [1,2]. The entropy of solid–solid phase transitions is much larger than of solid–liquid, and follows the Timmermans law [3]. There are few known crystals that exhibit this solid state energy storage property. In order to develop more materials for practical applications, binary or ternary systems are sought [4–10]. Typically, the low temperature phases have layered or chained tetragonal or monoclinic structures and transform to a cubic structure with orientational disorder [11,12]. In these layered/chained crystals, the O–H…O or O–H…N intermolecular bonds are rigid bonds in the low temperatures structures (designated as α or β phases), but in the high temperature (γ or γ'phase) structures these bonds rotate or oscillate around C–C bond in these tetrahedral globular molecules storing thermal energy. Some recent researches [13–15] about the dynamic disorder in a group of neopentane derivatives have been studied. There are only a few tetrahederally coordinated polyalcohol and amine organic crystals that store large amount thermal energy in orientationally disordered structure during solid–solid phase transitions of the first order. In order to increase availability of these materials with adjustable phase transition temperatures, binary mixtures are used. These are identified as thermal energy materials for applications in concentrated solar energy storage tower system, as secondary storage medium. These materials are becoming increasingly important as a renewable energy resource. Typical energies stroed in

* Corresponding authors.
E-mail addresses: dchandra@unr.edu (D. Chandra), jitendrasangwai@iitm.ac.in (J. Sangwai).

http://dx.doi.org/10.1016/j.calphad.2015.05.003
0364-5916/

the range of metals are negligible, as compared in solid state reactions of these materials.

In this study, we report on phase equilibria of binary 2-Amino-2-methyl-1, 3-propanediol (AMPL, $CH_3C(CH_2OH)_2NH_2$)- Tris(hydroxymethyl)aminomethane (TRIS, $C(CH_2OH)_3NH_2$) compounds, that are important for thermal energy storage applications. Rose et al. [16] reported the low temperature phase structure of AMPL to be monoclinic with lattice parameters; $a=8.62$ Å, $b=11.00$ Å, $c=6.10$ Å, $\beta=93.32°$, V=580.3 Å^3 at 293 K ($Z=4$). Chandra et al. [17,18] reported high temperature phase structure of AMPL as BCC with $a=6.7$ Å above ~357 K at which the hydrogen/nitrogen bond configuration changes and an isotropic but orientationally disordered BCC structure forms. It should be noted that polyalcohols, such as, pentaerythritol ($C_5H_{12}O_4$) [11], pentaglycerine ($C_5H_{12}O_3$) and others with tetrahedral C–C configuration and O–H…O bonds have FCC (γ or γ') high temperature structure whereas the amine compounds with O–H…N and O–H…O bonds, such as AMPL or TRIS have BCC obtained unlike most of the other plastic crystals which have FCC structure [5].

The low temperature phase structure of TRIS is the orthorhombic $Pn2_1a$ (space group 33) with four molecules per unit cell as reported by Eilerman and Rudman [19,20]. TRIS (in low temperature structure) forms layered structures perpendicular to the *c*-axis where hydroxyl groups are connected by strong hydrogen bonds within each layer and amine groups are connected by relatively weak hydrogen bonds between the layers with $a=8.844$ Å, $b=7.794$ Å, and $c=8.795$ Å. Kanesaka and Mizuguchi [21] studied the vibrational spectra of TRIS as a function of temperature in which the amino groups are oriented along the *c*-axis [21], and are involved only weakly in hydrogen bonding. The low to high temperature (β→γ') phase transition occurs at 403 K for the pure TRIS, and melting at 445 K [22].

In this study, low and high temperature solid solution phases that are rich in AMPL are designated as the "α and γ" and the phases rich in TRIS as "β and γ'" phases, respectively. Literature survey showed that the first experimental phase diagram was reported by Barrio et. al. [23] using differential scanning calorimetry data and X-ray diffraction data at three temperatures, 293 K, 335 K, and 378 K. They reported low [M+O] and high [C] temperature lattice parameters across the composition. The XRD data at 293 K and 335 K show coexistence of two low temperature [M+O] phases. At 378 K, (in Fig. 7 in Ref. [23]) the authors show a single high temperature [C] phase region up to 0.4TRIS, from their metastable quenched sample XRD data. Beyond 0.4TRIS composition they show a two phase region [C+O] at this temperature. We commend Barrio et al. [23] for their first attempt on producing the AMPL-TRIS phase diagram, and also reporting the high temperature BCC phase. However, demixing region of the two high temperature phases was not reported. In this study, we re-determined the phase diagram by performing in-situ x-ray diffraction (XRD as well as differential scanning calorimetric (DSC) studies, coupled with thermodynamic modeling based on CALPHAD [8] methodology to obtain optimized AMPL-TRIS phase diagram. The main difference between our new phase diagram and Barrio et al. [23] phase diagram is the high temperature region in which they show a single phase of orientationally disordered phase throughout the composition range, but we found that there are two high temperature phases, one rich in AMPL(γ) and the other rich in TRIS (γ′). In addition, thermodynamic calculation showed corroboration with our experimental data. We present experimental data collected over the range of composition, using in-situ x-ray diffraction, DSC complimented with thermodynamically modeled data for this AMPL-TRIS binary phase diagram study.

2. Experimental

AMPL (99% purity) and TRIS (99.99% ultra-high purity) were procured from Sigma-Aldrich and were used without any further purification, except heating for possible moisture removal. The AMPL and TRIS mixture binary samples are prepared at various compositions, and all compositions are reported as mole% in this paper. We follow a protocol in which the sample powders are premixed and melted in test tubes. Generally, the solidified melt does not give an equilibrium mixture of solid phases due to supercooling, and high temperature phases are retained at room temperature. To avoid this, we use strain induced transformation method in which equilibrium phases are attained. The methodology involves placing the binary mixtures in a freezer (~253 K) for 12 h, and then subject them high strain in a small cylinder with a piston; this method work well to obtain equilibrium crystal structures at room temperature. Differential scanning calorimetric (DSC) measurements were made to first obtain a major phase transition temperatures, deduce the compositions of eutectics/eutectoids etc., and finally the enthalpies of phase transitions were obtained. A TA Instruments DSC Q100 (TA instrument, USA) was used for this purpose. Sample sizes of 2–5 mg and the heating rate of 5 °C/min were used for this study. To confirm structures of the equilibrium phases, in-situ high temperature X-ray diffraction studies were performed on AMPL, TRIS and their binary solid solutions by using PANalytical X'Pert PRO diffractometer (PANalytical, Netherlands). Two sets of experiments were performed; one with samples in an Anton Paar heating XRK 900 stage (rate of 5 °C/min) with Argon purge gas, and the other using the capillary with the heated system that was mounted on the PANalytical diffractometer. The samples were sealed in a sapphire capillary. XRD patterns were obtained at various temperatures, and data were analyzed using X'Pert HighScore and MDI Jade computer programs to determine the phase transformation and crystal structures.

3. Results and discussions

3.1. Experimental results

In-situ high temperature X-ray diffraction (XRD) and DSC studies were used to determine the phase transformations of pure AMPL and TRIS, as well as their mixtures. X-ray diffraction patterns of pure AMPL taken at different temperatures as well as DSC scans are shown in Fig. 1. The low temperature α-AMPL phase of pure AMPL shows all the Bragg peaks at 308 K (35 °C) and 350 K (77 °C) (Fig. 1(a)). As the temperature is increased, the α-AMPL→γ-AMPL phase transition occurs at 357 K (84 °C) and Bragg peaks of the γ-AMPL high temperature BCC orientationally disordered phase appear at 359 (86 °C)–369 K (96 °C) XRD patterns (Fig. 1(a)). At 387 K (114 °C), we did not observe any Bragg peak, suggesting liquid phase formation. The DSC pattern for AMPL is shown in Fig. 1 (b). For pure AMPL, the solid–solid state phase transition (α-AMPL→γ-AMPL) occurs at 352 K (79 °C), and melts at 381 K (108 °C). The enthalpies of α-AMPL→γ-AMPL phase transformation are $\Delta H_{S\text{-}S}=226.1$ J/g, and $\Delta H_{S\text{-}L}=21.78$ J/g for γ-AMPL→liquid phase transformation. The transitions may be summarized as follows: $\alpha \underset{352k}{\rightarrow} \gamma \underset{381k}{\rightarrow} L$. In a similar manner XRD and DSC scans for pure TRIS are shown in Fig. 2. Fig. 2(a) shows in-situ XRD patterns of the low temperature β-TRIS phase at 308 K (35 °C) and 397 K (124 °C), and the γ′-TRIS high temperature BCC orientationally disordered phase at 406 K(133 °C) and 438 K(165 °C). The liquid phase forms at 445 K (172 °C). The transition temperatures match those obtained in the DSC pattern for TRIS (Fig. 2(b)). and may be summarized as: $\beta \underset{405k}{\rightarrow} \gamma' \underset{445k}{\rightarrow} L$ The enthalpies of β-TRIS→γ′-TRIS

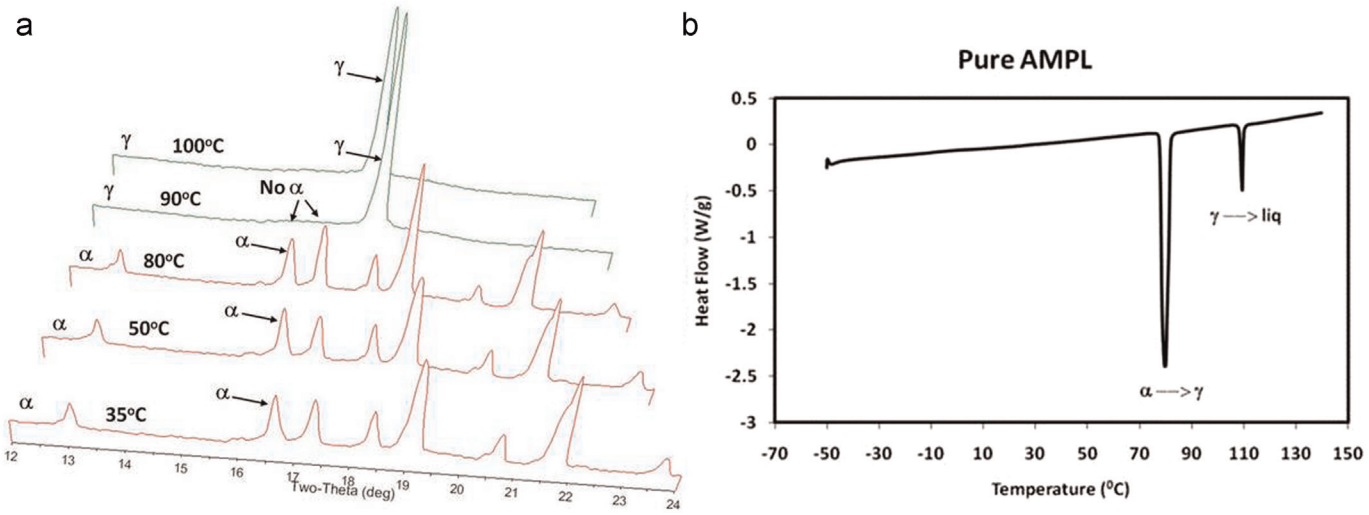

Fig. 1. (a) X-ray diffraction patterns of AMPL between 308 K (35 °C) and 369 K (96 °C) show α-AMPL, γ-AMPL at different temperatures in 3D. DSC pattern of AMPL is shown in (b).

phase transformation are $\Delta H_{S\text{-}S}=267.7$ J/g, and $\Delta H_{S\text{-}L}=26.47$ J/g for γ′-TRIS→liquid phase transformation.

Next we present phase transitions occurring in binary AMPL-TRIS system at 333 K (60 °C) and 373 K (100 °C) in Fig. 3. As the composition of TRIS is increased from 20% to 80%TRIS, the low temperature monoclinic α-AMPL and orthorhombic β-TRIS phases are stable at 333 K (60 °C); the XRD pattern of pure AMPL at 333 K (60 °C) is also in this Fig. 3(a). In the TRIS rich regions (90%TRIS), the Bragg peaks of only the β phase are observed (Fig. 3(a)). At higher temperature, for example at 373 K (100 °C), the orientational disordered γ-AMPL phase is observed for the compositions from 0% to 80% TRIS. The γ phase is stable for the 10%TRIS sample, and α-AMPL+γ-TRIS phases are stable for the compositions 30–80%TRIS, and only β phase is observed for the 90% TRIS as shown in Fig. 3(b). We performed more in-situ XRD work at various temperatures and compositions on many more solid solutions to confirm the stable phase regions in the phase diagram, but not shown here.

To verify existence of two high temperature phases, one rich AMPL (γ phase) and the other TRIS (γ' phase) in-situ x-ray diffraction patterns are obtained using sapphire capillary system for the 60%AMPL-40%TRIS (Fig. 4). In the case of 60%AMPL-40%TRIS, the AMPL-rich α-phase and TRIS-rich β-phase Bragg peaks can be observed up to 348 K (75 °C) (Fig. 4 (a)), and in the temperature range of 350 K (77 °C)–378 K (105 °C) the β+γ phases are stable. At 388 K (115 °C), the γ and γ' phase Bragg peaks are observed, (just above eutectoid temperature of β+γ→γ'in the phase diagram). These two high temperature phases were also observed in the x-ray diffraction patterns of 60%AMPL-40%TRIS composition as well; thus establishing the γ +γ' phase region above eutectoid temperature of 390 K (117 °C). Due to orientational disorder we observe only one strong Bragg peak of γ or γ' phase, referred to as "Plastic" phases in which the latent thermal heat energy is stored. The XRD patterns for γ(110) and γ'(110) Bragg peaks are shown in Fig. 4(a) and (c). At 403 K (130 °C), we observed L+γ' phase phases, and at 418 K (145 °C), we do not observe any Bragg peaks, so we conclude this to be Liquid phase region. The DSC plot of 60% AMPL-40%TRIS is also shown in Fig. 4(b). Based on XRD patterns, the phase transitions in 60%AMPL-40%TRIS composition sample are summarized as follows:

3.2. Proposed experimental phase diagram of AMPL-TRIS

The experimental phase diagram is developed by using XRD and DSC results. DSC results obtained from several compositions of AMPL-TRIS solutions are shown in Fig. 5. Table 1 shows phase transition temperatures and enthalpies obtained from these DSC plots. Fig. 5 shows α+β phases are stable up to ~348 K for

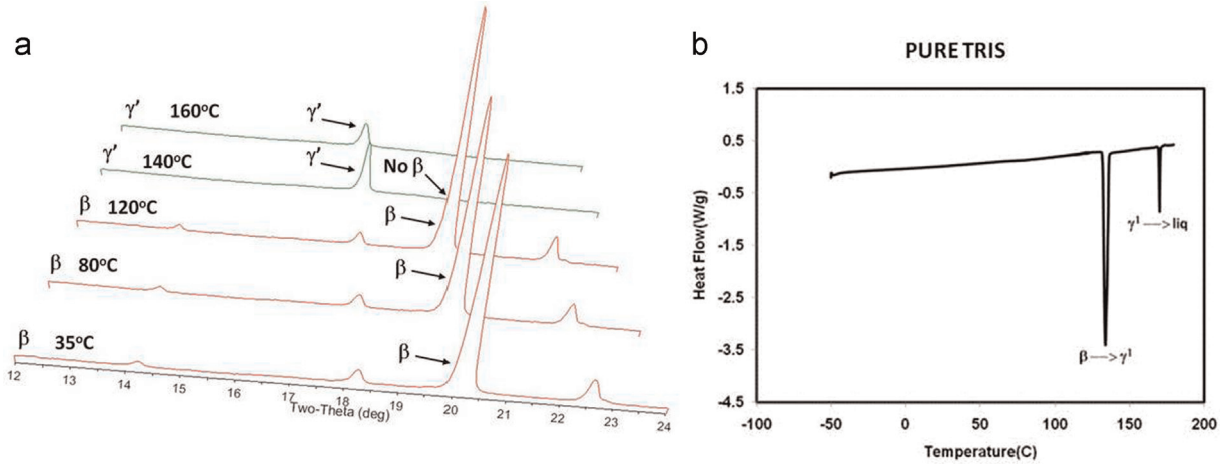

Fig. 2. (a) X-ray diffraction patterns of TRIS taken at 308–438 K that show β-TRIS, γ'-TRIS at different phase regions in 3D. The DSC pattern of TRIS is shown in (b).

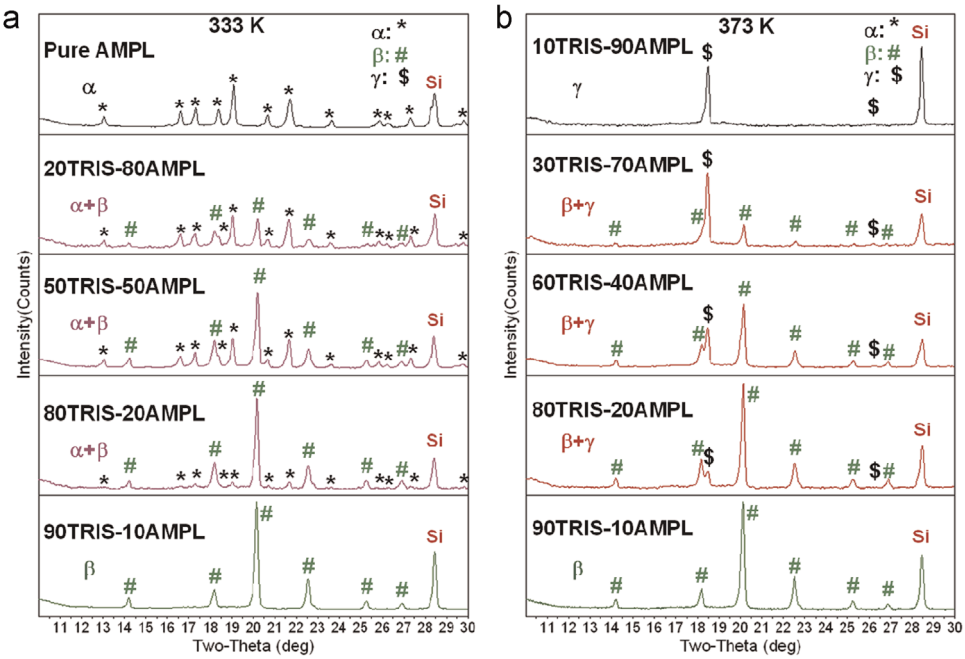

Fig. 3. X-ray diffraction patterns of solid solutions of AMPL-TRIS taken at 333 K and 373 K show α-AMPL, β-TRIS, γ-AMPL, α+β and β+γ different phase regions.

compositions 10–80%TRIS, pure γ-AMPL phase is stable up to 401 K leading to the peritectic γ→L+γ' phase at 404 K. The β+γ phases are stable up to 388 K. For the 90% and pure TRIS occurs at 405 K, and pure TRIS at 407 K. Other complex phase transitions for γ+γ' phases and others are determined x-ray diffraction method.

The solid–solid (S–S) phase transition in pure TRIS occurs at 407 K, whereas in pure AMPL it occurs at 353 K. We observe α→γ transitions for compositions between 10% and 80%TRIS at 348 K; it is clear that there are no significant changes in the S–S phase transition temperatures by adding TRIS to AMPL. However, the enthalpies of the S–S phase transition decreased from 194.8 J/g to 2.16 J/g as the concentration of %TRIS increased from 10% to 80% TRIS. The endothermic peaks observed at ~348 K in the DSC plots are mainly from molecules of AMPL during α-AMPL→ γ-AMPL, as the concentration of AMPL molecules decreases and TRIS molecular concentration increases, in the α+β region, we observe lower enthalpy of α→γ transition as the thermal energy is stored in these O–H…O or O–H…N bond rotations in AMPL molecules only. Note that the TRIS molecules are still in the low temperature β-phase, and are not participating the transitional energy storage.

Our proposed experimental AMPL-TRIS binary phase diagram is shown in Fig. 6. We will now describe phase transitions from low to high temperatures in this phase diagram. In the AMPL-rich region, the α→α+γ→γ phase transitions occur only up to 8%TRIS. Greater than 8–12%TRIS (eutectoid composition) α+β→α+γ→γ occur. The α+β→β+γ→γ are observed between 12% and 34% TRIS. In the mid-composition region, from 34% to 54%TRIS, the α+β→β+γ→γ+γ' occurs, and the α+β→β+γ→β+γ'→γ'phase transitions are observed from 54 to 89%TRIS. In the TRIS-rich region, β→β+γ'→γ'phase transitions are observed from 89% to 100%TRIS. In the high temperature region, the γ' single phase is stable from 54% to 100%TRIS (389–445 K). The L+γ phase region is stable from 0 to 38%TRIS, up to 401 K. The L+γ' phase region is stable between 22% and 100%TRIS (401–445 K).

The high temperature eutectoid reaction γ'(TRIS)→β(TRIS)+γ (AMPL) is observed with invariant point 388 K and 54%TRIS. The low temperature eutectoid reaction γ(AMPL)→α(AMPL)+β(TRIS) is observed with invariant point 348 K and 12%TRIS. A peritectic reaction, L+γ'(TRIS)→γ(AMPL), is observed with invariant point 401 K and 38%TRIS.

Barrio et al. [23] reported the γ→α+β eutectoid reaction at the 17%TRIS and the eutectoid temperature of 346 K; also reported α+β two phase region from 1%TRIS to 93%TRIS. In addition, they reported a large single phase BCC high temperature phase region between 0% and 100%TRIS (designated as [C] in their phase diagram) from 0% to 100% TRIS. But our phase diagram showed two separate γ and γ' regions, and a bounding (γ+γ') phase region between 34% and 54%TRIS (388–401 K); this is the main difference between our and Barrio et al. [23] phase diagram.

3.3. Thermodynamic Modeling-calculated AMPL-TRIS binary phase diagram by CALPHAD method

General aspects of CALPHAD thermodynamic modeling used in this work are described by Chellappa et al. [5,6]. We assigned the low temperature phases as α (AMPL rich) and β (TRIS rich), the high temperature phases are as γ (AMPL), γ' (TRIS), and the liquid phase as L. The notation "A" is for AMPL and "B" is for TRIS. The Gibbs energy of a phase ϕ (ϕ=α, β, γ, γ' or L) can be given as:

$$G^{\varnothing} = x_A {}^{\circ}G_A^{\varnothing} + x_B {}^{\circ}G_B^{\varnothing} + RT\left[x_A \ln(x_A) + x_B \ln(x_B)\right] + G^{EX,\varnothing} \quad (1)$$

where, x_A is the mole fraction of A, x_B is the mole fraction of B and R is equal to 8.314 J/mol K. ${}^{\circ}G_A^{\alpha}$ and ${}^{\circ}G_B^{\beta}$ are the Gibbs energies of pure components A and B in phase ϕ. $G^{EX,\phi}$ is the excess Gibbs energy. The Gibbs energies of α and β phases are chosen as reference states for pure components A and B, respectively. These two reference state Gibbs energies, ${}^{\circ}G_A^{\alpha}$ and ,${}^{\circ}G_B^{\beta}$ are set to be zero. All other stable and metastable modifications of pure components Gibbs energies are represented as changes from these reference states. The Gibbs energies for α and β phases can be written as:

$${}^{\circ}G_{AMPL}^{\alpha} = 0 \; and \; {}^{\circ}G_{TRIS}^{\beta} = 0 \quad (2)$$

The Gibbs energies for stable high temperature γ and γ' phases can be represented in term of reference states as:

$${}^{\circ}G_{AMPL}^{\gamma} = {}^{\circ}G_{AMPL}^{\alpha} + \Delta {}^{\circ}G_{AMPL}^{\alpha\to\gamma} = \Delta {}^{\circ}G_{AMPL}^{\alpha\to\gamma} \quad (3)$$

$${}^{\circ}G_{TRIS}^{\gamma'} = {}^{\circ}G_{TRIS}^{\beta} + \Delta {}^{\circ}G_{TRIS}^{\beta\to\gamma'} = \Delta {}^{\circ}G_{TRIS}^{\beta\to\gamma'} \quad (4)$$

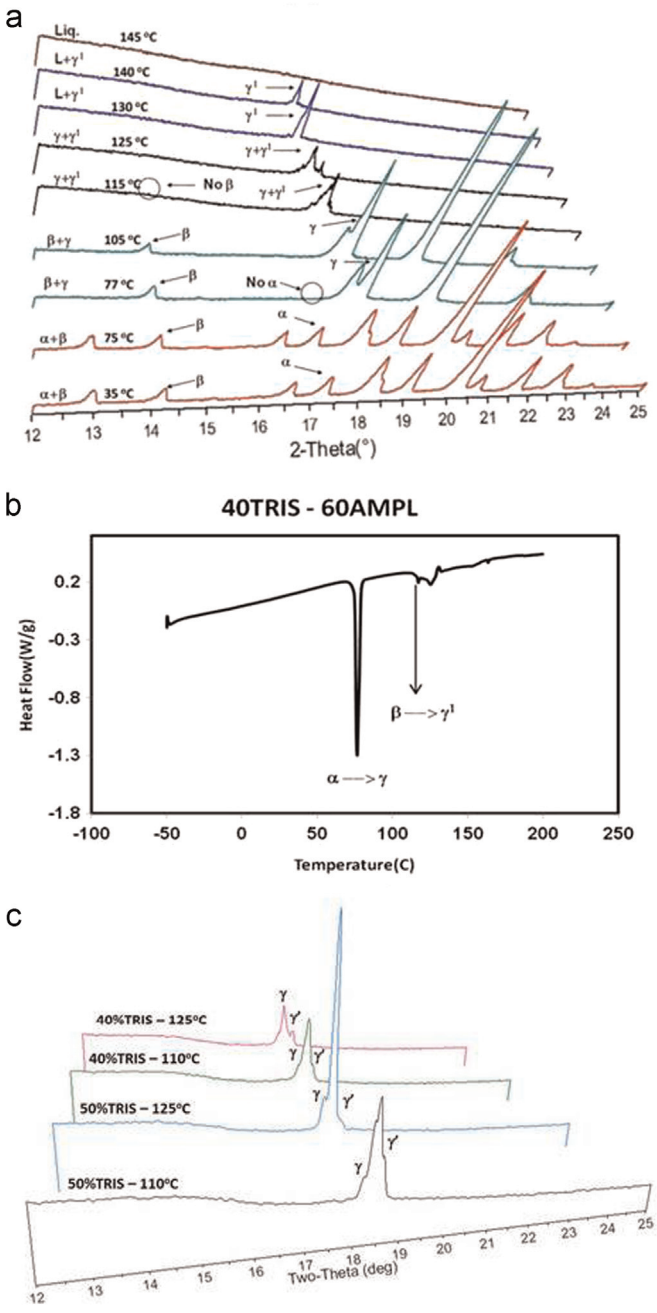

Fig. 4. (a) In-situ x-ray diffraction patterns of 60%AMPL-40%TRIS composition in a temperature range of 308 K (35°C) to 418 K(145 °C) showing presence of γ+γ' phases at 388 K(115 °C) and 398 K (125 °C) in the 3 dimenional plot, (b) DSC pattern shows conformatory endothermic peaks showing phase transitions α→γ at 350 K (77 °C), β→γ at 388 K(115 °C) and γ→L 401 K (138 °C), (c) expanded view of the Bragg peaks of high temperature γ and γ' "plastic phases" in 60%AMPL-40%TRIS and 50%AMPL-50%TRIS compsotions at 388 K (115 °C) and 398 K (125 °C).

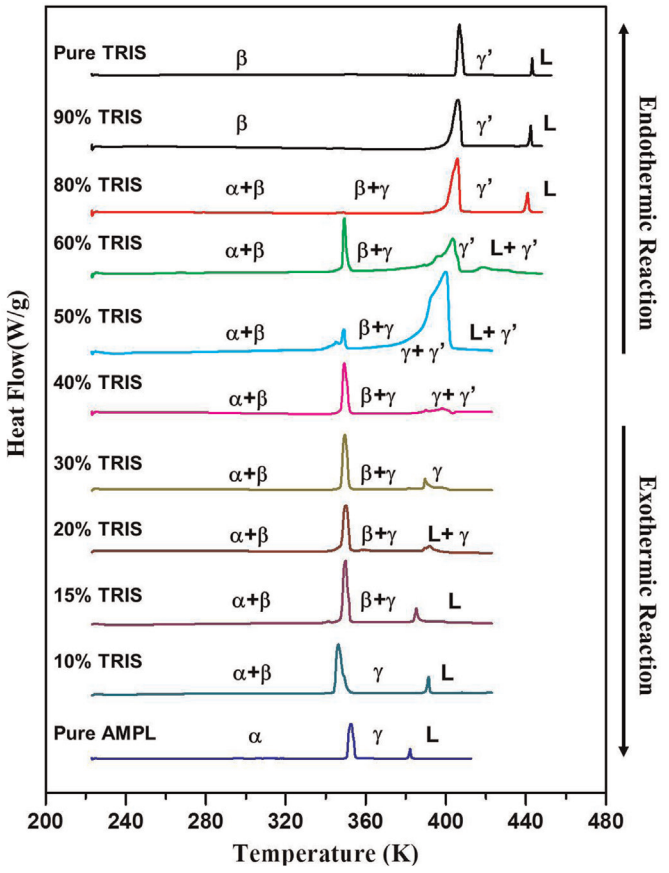

Fig. 5. Differential Scanning Calorimetric scans for various compositions of AMPL-TRIS binary solutions; these data along with the x-ray diffraction data are used in the experimentally determined phase diagram.

The Gibbs energies for the liquid phase can be written as:

$$^{\circ}G^{L}_{AMPL} = {}^{\circ}G^{\alpha}_{AMPL} + \Delta^{\circ}G^{\alpha\to L}_{AMPL} = \Delta^{\circ}G^{\alpha\to\gamma}_{AMPL} + \Delta^{\circ}G^{\gamma\to L}_{AMPL} \quad (5)$$

$$^{\circ}G^{L}_{TRIS} = {}^{\circ}G^{\beta}_{TRIS} + \Delta^{\circ}G^{\beta\to L}_{TRIS} = \Delta^{\circ}G^{\beta\to\gamma'}_{TRIS} + \Delta^{\circ}G^{\gamma'\to L}_{TRIS} \quad (6)$$

The pure component stable Gibbs energies, $^{\circ}G^{\gamma}_{AMPL}$, $^{\circ}G^{\gamma'}_{TRIS}$ $^{\circ}G^{L}_{AMPL}$, and $^{\circ}G^{L}_{TRIL}$, were determined including the heat capacity data proposed by Raja et al. [5] and Chandra et al. [24], and the expressions of the equations were described in Ref. [5]. Witusiewicz et al. [25] also developed the Gibbs energy parameters of AMPL in the form of GH^{SER}. However, we did not have the Gibbs energy parameters for TRIS in the same form as GH^{SER}. We tried to calculate the AMPL-TRIS phase diagram using Witusiewicz et al. [25] Gibbs energy data of AMPL and our TRIS data, but we could not generate the complete phase diagram. To calculate the Gibbs energy equations for the γ, γ' and the liquid phases of AMPL and TRIS, we use the heat capacity data from Refs. [5] and [24], and the general equations are given below:

$$^{\circ}G^{\gamma}_{AMPL} = \Delta^{\circ}G^{\alpha\to\gamma}_{AMPL} = \Delta H_{TR} - T\Delta S_{TR} + \int_{T_{TR}}^{T} \Delta C_P^{\alpha\to\gamma} dT - T\int_{T_{TR}}^{T} \frac{\Delta C_P^{\alpha\to\gamma}}{T} dT \quad (7a)$$

$$^{\circ}G^{\gamma'}_{TRIS} = \Delta^{\circ}G^{\beta\to\gamma'}_{TRIS} = \Delta H_{TR} - T\Delta S_{TR} + \int_{T_{TR}}^{T} \Delta C_P^{\beta\to\gamma'} dT - T\int_{T_{TR}}^{T} \frac{\Delta C_P^{\beta\to\gamma'}}{T} dT \quad (7b)$$

$$^{\circ}G^{L}_{AMPL} = \Delta^{\circ}G^{\alpha\to\gamma}_{AMPL} + \Delta^{\circ}G^{\gamma\to L}_{AMPL} = \Delta H_{TR} - T\Delta S_{TR} + \int_{T_{TR}}^{T} \Delta C_P^{\alpha\to\gamma} dT - T\int_{T_{TR}}^{T} \frac{\Delta C_P^{\alpha\to\gamma}}{T} dT + \Delta H_F - T\Delta S_F + \int_{T_F}^{T} \Delta C_P^{\gamma\to L} dT - T\int_{T_F}^{T} \frac{\Delta C_P^{\gamma\to L}}{T} dT \quad (8a)$$

Table 1
DSC results of pure TRIS, pure AMPL and their binary mixture sample.

Samples	1st S–S Phase transition		2nd S–S Phase transition		S–L Phase transition	
	T (K)	Enthalpies (J/g)	T (K)	Enthalpies (J/g)	T (°C)	Enthalpies (J/g)
Pure AMPL	353.2	236.8	–	–	384.6	28.4
10%TRIS	344.5	194.8	–	–	390.4	23.1
20%TRIS	347.9	161.6	388.6	33.4	–	–
30%TRIS	347.7	165.3	388.8	42.5	–	–
40%TRIS	347.9	123.9	388.7	35.8	–	–
50%TRIS	347.7	14.9	388.0	183.0	–	–
60%TRIS	348.3	49.3	397.4	108.1	–	–
80%TRIS	347.2	2.2	400.2	175.1	439.6	19.8
90%TRIS	401.4	242.8	–	–	441.6	23.4
Pure TRIS	407.0	285.0	–	–	445.2	27.8

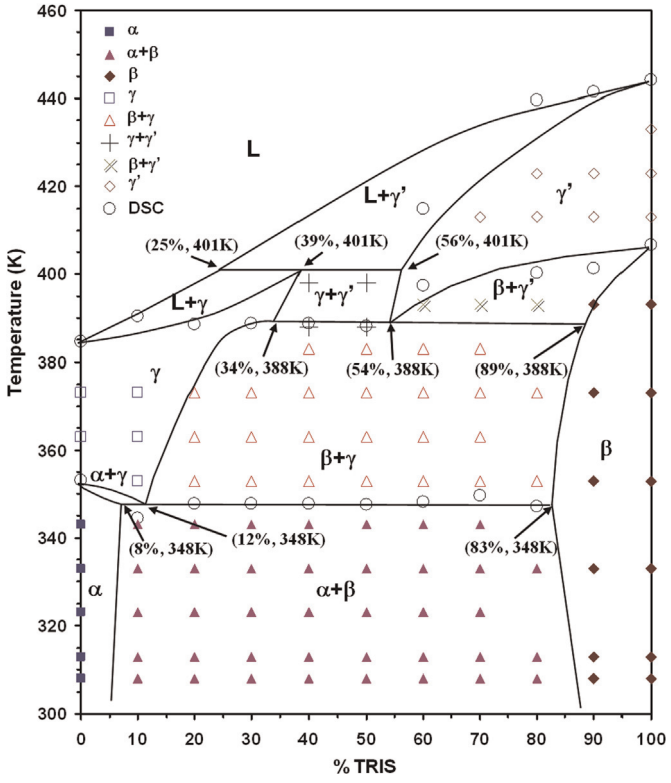

Fig. 6. Experimental phase from this study of AMPL-TRIS. The compositions of the key invariant and eutectic points, in addition to the phase boundaries are listed in parenthesis [X,Y: %TRIS, T(K)].

$$^{\circ}G^{L}_{TRIS} = \Delta^{\circ}G^{\beta\to\gamma'}_{TRIS} + \Delta^{\circ}G^{\gamma'\to L}_{TRIS}$$
$$= \Delta H_{TR} - T\Delta S_{TR} + \int_{T_{TR}}^{T} \Delta C_p^{\beta\to\gamma'} dT - T\int_{T_{TR}}^{T} \frac{\Delta C_p^{\beta\to\gamma'}}{T} dT$$
$$+ \Delta H_F - T\Delta S_F + \int_{T_F}^{T} \Delta C_p^{\gamma'\to L} dT - T\int_{T_F}^{T} \frac{\Delta C_p^{\gamma'\to L}}{T} dT \quad (8b)$$

Similar expressions can be obtained for Gibbs energies of stable phase for component "TRIS." The assumption that α, β, γ, and γ' phases are ideal solutions is used only to describe the metastable pure Gibbs energies which was described in reference [8]. The nature of non-ideality of theses phases can still be expressed as the sub-regular or regular solution model for the excess Gibbs energy ($G^{EX,\phi}$) which can be expressed as $G^{EX,\phi} = x_A x_B\left[L_0^{\phi} + L_1^{\phi}(x_A - x_B)\right]$, where the $L_0^{\phi}$and L_1^{ϕ} are the excess Gibbs energy parameters, the$L_0^{\phi}$and L_1^{ϕ} parameters can be temperature dependency or not, and they are optimized by using the PARROT module of THERMO-Calc software.

The phase transition temperatures (T_{TR} and T_F), enthalpies (ΔH_{TR} andΔH_F), and entropy (ΔS_{TR} and ΔS_F) for pure AMPL and TRIS are listed in Table 2 [4,5]. These parameters are used to calculate the phase diagram. Also, the experimental Cp data from the literature [5,24] are used to calculate the Gibbs energies for each phase and are given in Eq. (3) through (8). The interaction parameters are obtained from the PARROT program that gives the excess Gibbs energies that are listed in Eqs. (10) through (14). The expressions of Gibbs energies for the stable and metastable phases are listed in Table 3.

In this study, the optimized excess Gibbs energy parameters were determined using the following form of a power series:

$$L_m^{\varnothing} = a + bT + cTln(T) + dT^2 + eT^{-1} + fT^3 + gT^7 + hT^9 \quad (9)$$

Where *a*, *b*, *c*, *d*, *e*, *f*, *g*, and *h* are the excess Gibbs energy parameters. In most cases, only the first two terms of the above equation are used.

Expressions of Excess Gibbs Energies after optimization:

$$G^{EX,\alpha} = X_{AMPL}X_{TRIS}(3754.19558 - 2.2643398{*}T) \quad (10)$$

$$G^{EX,\beta} = X_{AMPL}X_{TRIS}(8600.52699 - 24.9684573{*}T) \quad (11)$$

$$G^{EX,\gamma} = X_{AMPL}X_{TRIS}\big((-9006.66041 + 28.9844832{*}T) + 183.063569{*}(X_{AMPL} - X_{TRIS})\big) \quad (12)$$

Table 2
Crystal structure, transition temperatures and thermal properties of AMPL and TRIS.

Compound	α or β phases	T_{TR} (K)	ΔH_{TR}(J mol^{-1})	ΔS_{TR}(J mole^{-1} K^{-1})	γ or γ' phases	T_F(K)	ΔH_F(J mol^{-1})	ΔS_F(J mole^{-1} K^{-1})	Reference
AMPL	Monoclinic	353	24902	70.5	BCC	385	2981	7.8	This study
		353	23300	66.0		385	2991	7.8	[26]
TRIS	orthorhombic	407	34531	84.8	BCC	445	3367	7.6	This study
		408	32690	80.1		445	3340	7.5	[4]
		407	34262	84.2		442	3041	6.9	[26]

Table 3
Expressions of Gibbs energies of pure components that includes heat capacity data.

Nos.	Gibbs energy expression
1	(s) $^{\circ}G^{\alpha}_{AMPL}$=0
2	(s) $^{\circ}G^{\beta}_{TRIS}$=0
3	(m) $^{\circ}G^{\beta}_{AMPL}$=4696.682
4	(m) $^{\circ}G^{\alpha}_{TRIS}$=5332.985
5	(s) $^{\circ}G^{\gamma}_{AMPL}$ = 24901.89 − 70.47*T − 0.275*T^2 + 949.46*T − 73097.48 − 110*T* LN(T)
6	(s) $^{\circ}G^{\gamma'}_{TRIS}$=34530.6 − 84.8*T − 0.461*T^2 + 1106.01*T − 119210.26 − 104.094*T* LN(T)
7	(m) $^{\circ}G^{\gamma'}_{AMPL}$=24901.89 − 70.47*T − 0.275*T^2 + 949.46*T − 73097.48 − 110*T* LN(T) + 1064.543
8	(m) $^{\circ}G^{\gamma}_{TRIS}$=34530.6 − 84.8*T − 0.461T^2 + 1106.01*T − 119210.48 − 104.094*T* LN(T) + 833.6818
9	(s) $^{\circ}G^{L}_{AMPL}$ = 27883.18 − 78.22*T − 0.29*T^2 + 1026.62*T − 78953.71 − 119.436*T* LN(T)
10	(s) $^{\circ}G^{L}_{TRIS}$=37897.64 − 92.36*T − 0.4085*T^2 + 730.07*T − 88174.84 − 57.714*T* LN(T)

$$G^{EX,\gamma'} = X_{AMPL}X_{TRIS}\left((-14730.8659 + 41.5885940*T) + 108.8016*(X_{AMPL} - X_{TRIS})\right) \quad (13)$$

$$G^{EX,L} = X_{AMPL}X_{TRIS}\left((4555.46420 - 1.23*T) - 1350.15434*(X_{AMPL} - X_{TRIS})\right) \quad (14)$$

The excess Gibbs energy Eqs. (12) and (13) The compensation temperatures for these two orientationally disordered γ and γ′ phases at the equimolar composition (X=0.5) are calculated as $T_c = H^{ex}/S^{ex} =$ 310 K and 354 K from Eqs. (12) and (13) [26], where $G^{EX,\gamma}$=0 *and* $G^{EX,\gamma'}$=0. These are very close to the value reported by Lopez et al. [27,28]. From a thermodynamic point of view, this optimization for these two orientationally disordered γ and γ′ phases as BCC present similar excess properties."

The optimized AMPL-TRIS binary phase diagram is shown in Fig. 7. The comparison between the experimental and calculated invariant equilibria is given in Table 4. The first eutectoid (γ→α+β) point is at 17%TRIS and 348.4 K for the calculated phase diagram. This result is closed to our experimental phase diagram which is at 12%TRIS and 348 K, and Barrio et al. result at 17%TRIS and 346 K. The γ'→β+γ and L+γ'→γ reactions are reported in Barrio et al. [23] experimental phase diagram. Another eutectoid (γ'→β+γ) point is calculated at 55%TRIS and 388 K which is closed to our experimental result (54%TRIS and 388 K). The calculated peritectic temperature is close to our experimental temperature of 401 K, however the calculated peritectic composition (36%TRIS) is 3% lower than our experimental composition.

4. Conclusions

The proposed AMPL-TRIS binary phase diagram has been experimentally developed and calculated using CALPHAD method, and we find good correspondence between these two phase diagrams. We determined two high temperature γ-AMPL and γ'-TRIS

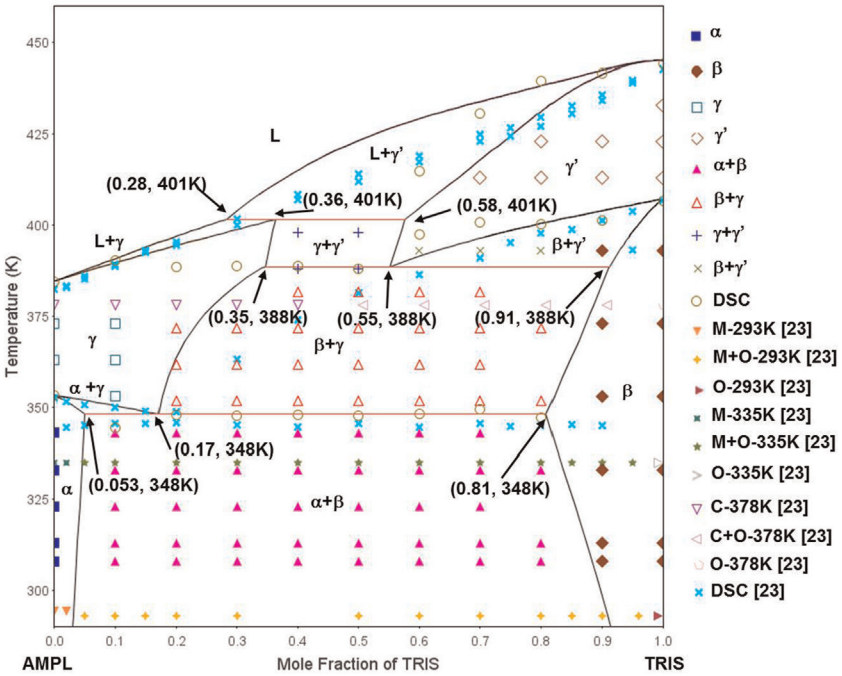

Fig. 7. CALPHAD modeled and optimized AMPL–TRIS binary phase diagram.

Table 4
Comparison of calculated and experimental invariant equilibria.

Invariant Equilibria		X_{TRIS} (mole fraction of TRIS)			Temperature (K)
		α	γ	β	
γ→α+β	(E)	0.08	0.12	0.83	348
(Eutectoid)	(E)	0.01[a]	0.17[a]	0.93[a]	346[a]
	(C)	0.053	0.17	0.81	348
		γ	γ'	β	
γ'→β+γ	(E)	0.34	0.54	0.89	388
(Eutectoid)	(C)	0.35	0.55	0.91	388
		L	γ	γ'	
L+γ'→γ	(E)	0.25	0.39	0.56	404
(Peritectic)	(C)	0.28	0.36	0.58	401

[a] Experiment data from Barrio et al. [23]. No γ'→β+γ and L+γ'→γ reactions reported by Barrio et al. [23] E: experiment, C: calculation.

phases present in this phase diagram; these are orientationally disordered BCC structure. We have found these in other poly-alcohol systems. Also there is a γ+γ′region present. There are two eutectoids transformations; one with invariant point 348 K and 12%TRIS, where γ→α+β, and the other with invariant point 388 K and 54%TRIS where γ′→β+γ. One peritectic is observed with invariant point 401 K and 38%TRIS where γ→L+γ. The low temperature α-AMPL+β-TRIS phases are stable up to 348 K. It is interesting that the γ phase is stable up to 348 K even in the TRIS rich region, and up to 415 K in the AMPL region, whereas the γ'phase is stable greater than 388 K. Both pure and binary solid solutions show that these organic compounds can store more thermal energies during solid–solid state phase transformation as compared to solid–liquid phase transformation.

Conflict Of Interest

There are no conflicts of interest.

Appendix A. Supplementary material

Supplementary data associated with this article can be found in the online version at http://dx.doi.org/10.1016/j.calphad.2015.05.003.

References

[1] Dirk Jörg Reuter, Josep Ll Büsing, Tamarit, Albert Würflinger, High-pressure differential thermal analysis study of the phasebehaviour in sometert-butyl compounds: pivalic acid,2-methylpropane-2-thiol and tert-butylamine, J. Mater. Chem. 7 (1997) 41–46.

[2] J. Ll Tamarit, I.B. Rietveld, M. Barrio, R. Céolin, The relationship between orientational disorder and pressure: the case study of succinonitrile, J. Mol. Struct. 1078 (2014) 3–9.

[3] J. Timmermans, Plastic crystals: a historical review, J. Phys. Chem. Solids 18 (1) (1961) 1–8.

[4] Dhanesh Chandra, Raja Chellappa, Wen-Ming Chien, Thermodynamic assessment of binary solid-state thermal storage materials, J. Phys. Chem. Solids 66 (2005) 235–245.

[5] (a) Raja Chellappa, Renee Russell, Dhanesh Chandra, Thermodynamic modeling of the $C(CH_2OH)_4$–$(NH_2)(CH_3)C(CH_2OH)_2$ binary system, J. Comput. Coupling Phase Diag. Thermochem. **28** (2004) 3–8;
(b) Raja Chellappa, Dhanesh Chandra, Phase diagram calculations of organic "Plastic Crystal" binaries: $(NH_2)(CH_3)C(CH_2OH)_2$-$(CH_3)_2C(CH_2OH)_2$ system, Comput. Coupling Phase Diag. Thermochem. 27 (2003) 133–140.

[6] Raja Renee Russell, Chellappa, Dhanesh Chandra, Determination of the phase diagram of the binary system $C(CH_2OH)_4$–$(NH_2)(CH_3)C(CH_2OH)_2$ by high resolution guinier diffractometry and differential scanning calorimetry, CALPHAD 28 (2004) 41–48.

[7] A. Mishra, A. Talekar, D. Chandra, W.-M. Chien, , Ternary phase diagram calculations of pentaerythritol–pentaglycerine–neopentylglycol system, Thermochim. Acta 535 (2012) 17–26.

[8] Amrita Mishra, Anjali Talekar, Renhai Shi, Dhanesh Chandra, Thermodynamic assessment of orientationally disordered organic molecular crystals: Ternary system pentaerythritol – neopentylglycol – 2-amino-2methyl-1,3,propanediol (PE–NPG–AMPL), J. Comput. Coupling Phase Diagr. Thermochem. 46 (2014) 108–117.

[9] M. Barrio, J. Font, D.O. López, J. Muntasell, J.Ll Tamarit, Floor radiant system with heat storage by a solid-solid phase transition material, Sol. Energy Mater. Sol. Cells 27 (2) (1992) 127–133.

[10] M. Barrio, J. Font, J. Muntasell, J. Navarro, J.Ll Tamarit, Applicability for heat storage of binary systems of neopentylglycol, pentaglycerine and pentaerythritol: a comparative analysis, Sol. Energy Mater. 18 (1–2) (1988) 109–115.

[11] Isamu Nitta, Tokunosuke Watanabe, X-Ray investigation of the cubic modification of pentaerythritol, $C(CH_2OH)_4$, Bull. Chem. Soc. Jpn. 13 (1) (1938) 28–35.

[12] Cynthia S. Dhanesh Chandra, Day, Charles S. Barrett, Powder Diffr. J 8 (02) (1993) 109–117.

[13] Aleksandra Drozd-Rzoska, Sylwester J. Rzoska, Sebastian Pawlus, Josep Ll Tamarit, Phys. Rev. B 73 (22) (2006) 224205.

[14] J. Ll Tamarit1,3, D.O. López1, M.R. de la Fuente2, M.A. Pérez-Jubindo2, J. Salud1, M. Barrio1, J. Phys.: Condens. Matter 12 (37) (2000) 8209–828220.

[15] J. Ll Tamarit, M.A. Pérez-Jubindo, M.R. de la Fuente, J. Phys. Condens. Matter 9 (25) (1997) 5469–5478.

[16] H.A. Rose, A. Van Camp, Anal. Chem. 28 (11) (1956) 1790–1791.

[17] (a) D. Chandra, W. Ding, R.A. Lynch, J.J. Tomlinson, Phase transitions in plastic crystals, J. Less Common Met. 168 (1) (1991) 159 67.;
(b) D. Chandra, R.A. Lynch, W. Ding, J.J. Tomlinson, Advances in X-Ray analysis, Plenum Publishing (1989), p. 609–615.

[18] J.H. Helms, A. Majumdar, D. Chandra, AC conductivities of neopentylglycol and 2-amino-2-methyl-1,3- propanedi, J. Electrochem. Soc. 140 (4) (1993) 1048–1055.

[19] Donna Eilerman, Reuben Rudman, Polymorphism of crystalline poly(hydroxymethyl) compounds. III. The structures of crystalline and plastic tris(hydroxymethyl)aminomethane, J. Chem. Phys 72 (10) (1980) 5656–5666.

[20] R. Rudman, D. Eilerman, Science 200 (1978) 531–532.

[21] I. Kanesaka, K. Mizuguchi, , Vibrational study of hydrogen bonds and structure of tris(hydroxymethyl)aminomethane, J. Raman Spectrosc. 29 (9) (1998) 813–817.

[22] S. Schroetter, D. Bougeard, J. Lascombe, Dynamics of Molecular Crystals, Elsevier, Grenoble, France (1986), p. 213.

[23] M. Barrio, J. Font, D.O. Lopez, J. Muntasell, J.L. Tamarit, Y.J. Haget, Plastic molecular alloys: The binary-system tris(hydroxymethyl) aminomethane 2-amino-2-methyl-1,3-propanediol, J. Chim. Phys. Physico-Chim. Biol. 91 (1994) 189–202.

[24] D. Chandra, W.-M. Chien, V. Gandikotta, D.W. Lindle, Z. Phys. Chem. 216 (2002) 1433.

[25] V.T. Witusiewicz, L. Sturz, U. Hecht, S. Rex, Thermodynamic description and unidirectional solidification of eutectic organic alloys: II.$(CH_3)_2C(CH_2OH)_2$–$(NH_2)(CH_3)C(CH_2OH)_2$ system, Acta Mater. 52 (2004) 5071–5081.

[26] E. Murrill, L. Breed, Thermochim. Acta 1 (1970) 239–246.

[27] D.O. Lopez, J. Salud, J.L.I. Tamarit, M. Barrio, H.A.J. Oonk, Uniform thermodynamic description of the orientationally disordered mixed crystals of a group of neopentane derivatives, Chem. Mater 12 (2000) 1108–1114.

[28] David O. Josep Salud, Josep Ll López, Maria Tamarit, Barrio, Harry A.J. Oonk, Two-component systems of isomorphous orientationally disordered crystals. Part 2 Thermodynamic analysis, J. Mater. Chem. 9 (1999) 917–921.